Mendeleev Communications

Mendeleev Commun., 2025, **35**, 732–735

Stereochemical analysis of natural products: alkaloids from the root bark of *Strychnos panganensis*

Dmitry A. Grigoriev,[a] Valentin A. Semenov,*[a] Luc Angenot,[b] Georges Massiot[c] and Leonid B. Krivdin[a]

[a] *A. E. Favorsky Irkutsk Institute of Chemistry, Siberian Branch of the Russian Academy of Sciences, 664033 Irkutsk, Russian Federation. E-mail: semenov@irioch.irk.ru*

[b] *Center of Interdisciplinary Research on Medicines, Faculty of Medicine, University of Liège, 4000 Liège, Belgium*

[c] *Institut de Chimie Moléculaire de Reims, UMR CNRS 7312, Université Reims-Champagne-Ardenne, UFR Sciences, 51100 Reims, France*

DOI: 10.71267/mencom.7827

The possibilities of reliable determination of spatial structures of natural products based on correlation of high-level calculated and experimental ^{1}H and ^{13}C NMR chemical shifts are considered using the example of four main representatives of the panganensine series, *Strychnos-Strychnos* type bisindole alkaloids. For isomeric panganensines X and Y, the reassignment of a number of individual NMR signals together with the spectral assignment of experimentally unresolved peaks is suggested, which allows the establishment of the absolute configuration for C-19, the only out-of-ring asymmetric carbon atom.

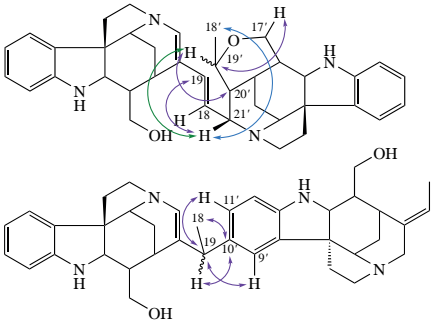

Keywords: indoles, alkaloids, panganensine, stereochemistry, computational NMR, DFT, ^{1}H and ^{13}C NMR spectra.

The present communication deals with the stereochemical analysis of natural bisindole alkaloids,[1,2] more precisely, a detailed structural analysis of four alkaloids **1**–**4** extracted from the root bark of *Strychnos panganensis* known as panganensines R, S, X and Y (Figure 1) is performed. Historically, panganensines **1**–**4** were identified as novel alkaloids in addition to known representatives of this series like matopensine. These alkaloids are characterized by their unique dimeric structure composed of two smaller alkaloid almost similar units linked together. In this pioneering communication, we have performed state-of-the-art stereochemical study of four most interesting classical representatives of this series by means of the original high-level DFT calculations of their ^{1}H and ^{13}C NMR chemical shifts, as compared to experiment.

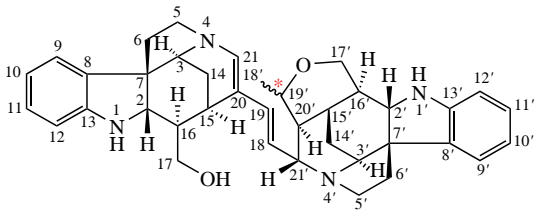

1 Panganensine R (19′*R*)
2 Panganensine S (19′*S*)

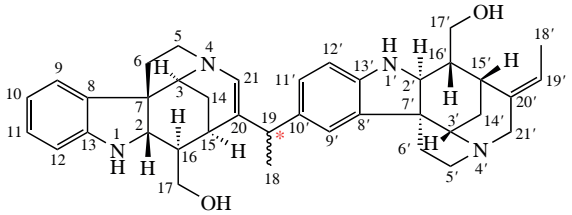

3 Panganensine X (19*S*)
4 Panganensine Y (19*R*)

Figure 1 Structures and atom numbering of panganensines **1**–**4**.

Plant *Strychnos panganensis* Gilg is a scrambling shrub or liana, 3–20 m climbing in trees (see Online Supplementary Materials). Panganensines S, X and Y evaluated against chloroquine-resistant and sensitive lines of *Plasmodium falciparum* exhibited moderate to weak activity with antiplasmodial IC_{50} values of 5–20 mM against *Plasmodium* lines.[3] The amount of isolated panganensine R was not sufficient for the pharmacological testing. The leaves of two East African specimens were screened for alkaloids but only traces have been found for one of the two.[4] On the other hand, the alkaloids of root bark of *Strychnos panganensis* collected in Tanzania were extracted and deeply studied at the University of Reims.[5] From 6.6 g fraction of crude alkaloids, twelve alkaloids were isolated. Among them six were new, among which dimeric indolinic alkaloids were named as panganensines R, S, X and Y. These alkaloids were made up of *N*-deacetylated retuline, isoretuline and spermostrychnine and it was soon realized that they were pairs of diastereoisomers. The first pair was named panganensines R and S, without knowing which was C-21′ *R* and C-21′ *S*. For the second pair, the letters X and Y were chosen and supposed to possess *R*- or *S*-configurations at C-19, respectively. With the tools available at that time, it was not possible to determine the missing configurations.

Thus, at the first stage of the present study, a preliminary conformational search was carried out to establish the spatial three-dimensional structures of **1**–**4**. It is worth noting that the entries for panganensines S and X in the PubChem database were deposited with incorrect designations of their three-

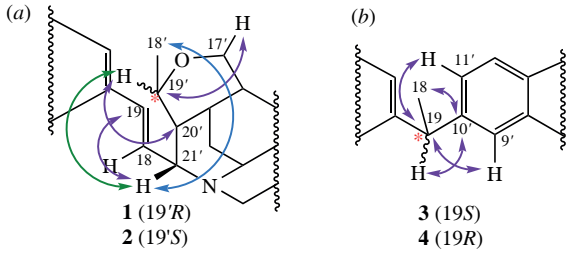

Figure 2 Principal NMR correlations of (*a*) compounds **1**, **2** and (*b*) compounds **3**, **4**. Violet arrows correspond to the {^{1}H–^{13}C} HMBC of **1**–**4**, the blue one is related to the {^{1}H–^{1}H} ROESY of **1**, while the green belongs to {^{1}H–^{1}H} ROESY of **2**.

dimensional structures.[6,7] At that point, the mutual arrangement of the subunits in each molecule was thoroughly investigated. Whenever possible, available experimental data extracted from the ROESY and HMBC correlations were taken into account (Figure 2).

Despite the minor structural differences of **1**–**4**, they demonstrate a marked influence of chemical structure on the variation of chemical shifts. Performed conformational search was reduced mainly to identifying the exact angles of rotation of subunits at the C-19–C-20 and C-18–C-21′ bonds in panganensines R and S, and those at the C-19–C-20 and C-19–C-10′ bonds in panganensines X and Y. The conformational search in the energy range of 0–10 kcal mol^{-1} relative to the detected minimum revealed several groups of conformers that corresponded to the stereochemical structures of compounds **1**–**4**, as it was initially established by a series of NMR experiments.[5]

As a result of molecular modeling, we selected from 4 to 6 groups from all identified low-energy conformers for each of the alkaloids under study. Here we present the results of the stereochemical analysis of **1**–**4** with a brief summary of the applied calculation procedures exemplified with the *S*-isomer of panganensine X (**3**) or Y (**4**) in more detail. At the initial stage of the conformational search, as many as six groups of the most favorable conformers **3a**–**f** were identified (Figure 3 and Online Supplementary Materials for details). For these conformers, the distribution of their relative free energies was found to be 2.1, 2.2, 3.8, 4.3, 0.0, and 4.1 kcal mol^{-1} when going from **a** to **f**. In the next step, geometric parameters of these six low-energy conformers were refined by the higher-level optimization at the M06-2X/pecG-2 level[8–10] in the liquid phase of chloroform-*d*.[11,12] Cartesian coordinates of main conformers of **1**–**4**, optimized in the liquid phase of chloroform, are given in the Online Supplementary Materials. Next, for the obtained optimized structures **3a**–**f**, all shielding constants were calculated together with the corresponding ^{1}H and ^{13}C NMR chemical shifts within the GIAO-PBE0/pecS-2 scheme[13–15] (see Online Supplementary Materials, Table S1). Both geometry optimization and chemical shift calculations were performed using accordingly new efficient basis sets pecG-2 and pecS-2,[16,17] which were optimized for the calculations of large synthetic organic molecules and natural products.

The obtained calculated values of NMR chemical shifts are compared with the known experimental data. Based on this comparison, on the one hand, a correlation assessment of the quality of the computational procedure is carried out, and on the other hand, the degree of correspondence (or non-correspondence) of the values of the resonance peaks of ^{1}H and ^{13}C of the experimental spectra to their theoretically obtained values is determined. This approach has proven itself well and is widely used in the interpretation of spectral parameters of natural compounds.[18] After comparing the theoretically calculated NMR chemical shifts with two experimental sets of signals for both the *R*- and *S*-isomers of panganensines X and Y (**3** and **4**, respectively), it became clear that X was the *S*- and Y was the *R*-isomer.

As for the piperidine conformation of the second subunit of panganensines X (**3**) and Y (**4**), the attached six-membered ring form a (3-3-1) system, which has a single constraint: the substituents at the ring junction should be *equatorial*, then the two six membered rings could be either *boat* or *chair*, even though another five-membered ring comes to pinch the system. As regards the piperidine ring and due to the five-membered ring which removes all mobility to the nitrogen atom, the only flexibility is in C-21′ (*axial* or *equatorial*). As regards the other six-membered ring, there is flexibility around the C-2′ to C-16′ bond and depending on configurations of these carbon atoms, there can be a *chair* or a *boat*. Up to now the sole conformation found for the piperidine ring of deacetylisoretuline is the *chair* form.[19] A *boat* form may exist in both rings and the only means to demonstrate its existence would be through the observation of NOEs (or ROEs) between either H-14′s and H-21′ or H-2′. Unfortunately, spectra are no longer available, and calculations are thus the only way to probe or not the existence of a second subunit piperidine in a *boat* form.

In this case, such statistical descriptors as the corrected mean absolute error (CMAE) and the root mean square deviation (RMSD) were used to assess the reliability of the obtained theoretical values. The results of the performed comparison of all calculated and experimental ^{1}H and ^{13}C NMR chemical shifts for the conformers of **1**–**4** are presented in Table S2. In addition, to increase the reliability of applied methodology, the DP4+ approach[20,21] was used. Using this technique to analyze the probability density distribution of the lowest-energy conformers of panganensine X (**3**), we concluded that the most probable conformer of this alkaloid was the one with a stereochemical structure close to that of **3b** (Table 1). It also followed from the performed DP4+ analysis that among all six possible conformers of panganensine X, **3b** was the most sustained, although it did not have the lowest energy. The probability density distribution diagrams of the conformers of three remaining alkaloids **1**, **2**,

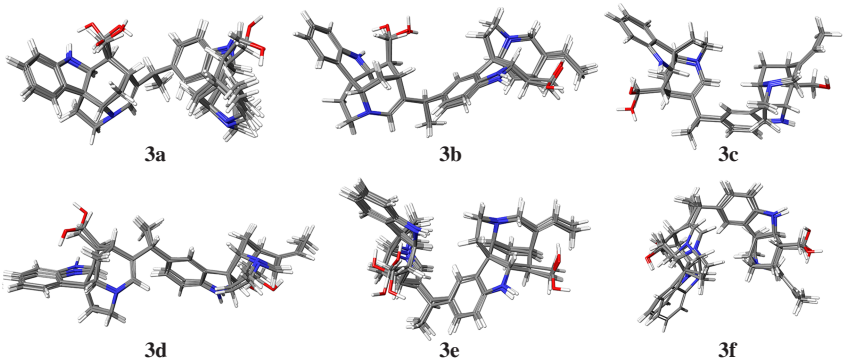

Figure 3 Three-dimensional structures of the main low-energy groups of conformers **3a**–**f** of panganensine X (**3**), optimized at the M06-2X/pecG-2 level.

Table 1 Graphs of the DP4+ probability distribution (%) of the main conformers **3a**–**f** of panganensine X, obtained by correlating calculated *vs.* experimental NMR data. Here *s*DP4+ denotes scaled values of DP4+ while *u*DP4+ denotes the unscaled DP4+ values.

Graph	Conformer					
	3a	**3b**	**3c**	**3d**	**3e**	**3f**
*s*DP4+ (^{1}H *data*)	0.0	99.9	0.0	0.0	0.0	0.0
*s*DP4+ (^{13}C *data*)	95.9	2.4	0.3	1.4	0.0	0.0
***s*DP4+ (*all data*)**	2.5	97.5	0.0	0.0	0.0	0.0
*u*DP4+ (^{1}H *data*)	0.0	100.0	0.0	0.0	0.0	0.0
*u*DP4+ (^{13}C *data*)	0.3	99.7	0.0	0.0	0.0	0.0
***u*DP4+ (*all data*)**	0.0	100.0	0.0	0.0	0.0	0.0
DP4+ (^{1}H *data*)	0.0	100.0	0.0	0.0	0.0	0.0
DP4+ (^{13}C *data*)	11.4	88.6	0.0	0.0	0.0	0.0
DP4+ (*all data*)	0.0	100.0	0.0	0.0	0.0	0.0

and **4** from this series are provided in Figure S1 (see Online Supplementary Materials).

In general, the average level of error for the calculation of ^{1}H and ^{13}C NMR chemical shifts in the whole series of alkaloids under study **1**–**4** is quite low (Table S2). For the **3b** conformer of panganensine X, the CMAE of calculated ^{1}H and ^{13}C chemical shifts was only 0.17 and 2.2 ppm, while RMSD was accordingly 0.21 and 3.1 ppm. All calculated and experimental ^{1}H and ^{13}C NMR chemical shifts of this conformer are presented in Figure 4. It should also be mentioned that among the provided chemical shifts of **3b**, there are some outlined deviations that do not fit into the overall correlation. All found deviations for the conformers **1a**, **2b**, **3b**, and **4c** are collected in Table 2 and discussed elsewhere in this paper.

Next, we will consider in more detail the results of the performed correlation analysis of the most favorable conformers of **1**–**4**. An excellent agreement between calculated ^{13}C NMR chemical shifts and their experimental values was reached for panganensine R (conformer **1a**). Unfortunately, no experimental data for C-18 and C-20 is available in the literature. The only significant deviation was found for C-15, which was probably due to the electronic effects propagated through the influence of the nearest C-20 atom participating in the conjugated π-system (see Table 2). As for the ^{1}H NMR chemical shifts, there are no experimental data for each second proton at C-6, C-17, and C-14′. Despite the fact that those protons are bonded in pairs to one carbon atom, their chemical shifts were expected to differ essentially. We have estimated all missing ^{1}H NMR chemical shifts based on the established correlation (Figure S2). A

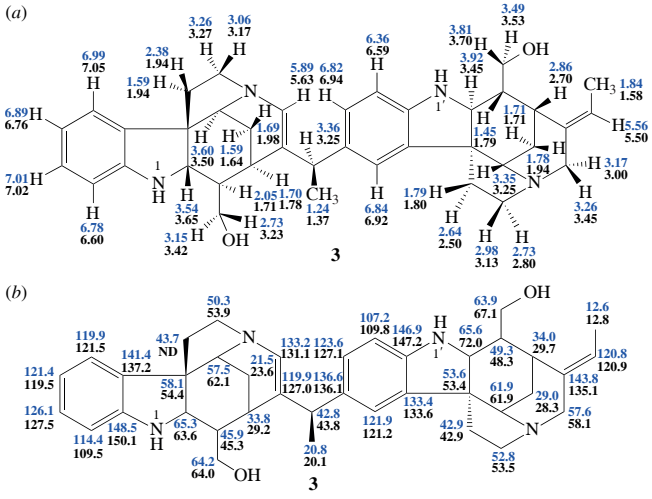

Figure 4 Calculated (blue) and experimental (black) (*a*) ^{1}H NMR and (*b*) ^{13}C NMR chemical shifts of **3** (calculated values are provided for the **3b** conformer, see Figure 3).

Table 2 Selected ambiguous cases of NMR chemical shifts (ppm) of the main conformers of **1**–**4**. Deviations of calculated values from experiment are given in parentheses.

Position	**1a**	**2b**	**3b**	**4c**
		^{1}H NMR		
2	3.83 (0.87)			
14 (b)				2.78 (0.88)
21				4.90 (0.85)
2′			3.92 (0.47)	
		^{13}C NMR		
15	30.8 (5.3)			35.3 (6.9)
19		134.8 (5.8)		
20			119.9 (7.1)	
21				137.1 (6.4)
2′			65.6 (6.4)	
20′			143.8 (8.7)	144.7 (10.4)

significant deviation of theoretical and experimental values for H-2 should be explained by its through-space intramolecular interaction involving the hydroxyl group at O-17 and formation of the five-membered ring involving hydrogen bonding between H-2 and oxygen atom.

No ^{13}C NMR data is available for the C-18 atom of panganensine S (conformer **2b**), so we used its theoretical estimation (see Figure S2). The most noticeable deviation from the overall correlation is observed for the C-19 atom, which is likely due to mixed electronic effects in the conjugation chain that cannot be taken into account in the stationary state. The ^{1}H NMR data show good agreement between calculated and experimental values of chemical shifts. In stereoisomer *S*, theoretical chemical shift H-2 fits into correlation trend quite well, indicating a less pronounced influence of the hydroxy group OH-17, as compared to that in panganensine R (**1**).

In the case of ^{13}C NMR chemical shifts of panganensine X (conformer **3b**), three significant deviations from the general correlation trend for atoms C-20, C-2′ and C-20′ were detected (Figure 5). The chemical shift of C-20, as in previous cases, is distinguished by a noticeable discrepancy between the experimental and calculated values (see Table 2). Apparently, this is due to the effect of delocalization of the electron density caused by the interaction of the N-4 lone pair with the π-system of C-20/C-21 double bond. To understand the origin of deviations for C-2′ and C-20′, as part of the calculation procedure we have performed a topological analysis of the electron density distribution for **3b** using the formalism of the QTAIM theory.[22] According to the results of the performed topological analysis in the cavity of the bowl-shaped nine-membered system C-2′–C-7′–C-6′–C-5′–N-4′–C-21′–C-20′–C-15′–C-16′ of the second subunit of **3b**, the localization of two bond critical points of the (3,–1) type was discovered (see Figure 5). It follows that the C-2′ atom reflects the influence of the intramolecular non-valent interaction with the hydroxyl group OH-17′ through H-2.

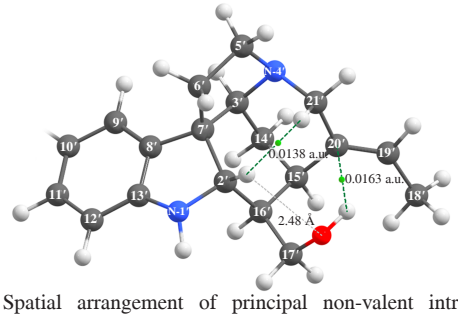

Figure 5 Spatial arrangement of principal non-valent intramolecular interactions and (3,–1) bond critical points in the second subunit of **3b** (bond critical points are shown as green circles with corresponding numerical values of electron density in a.u.).

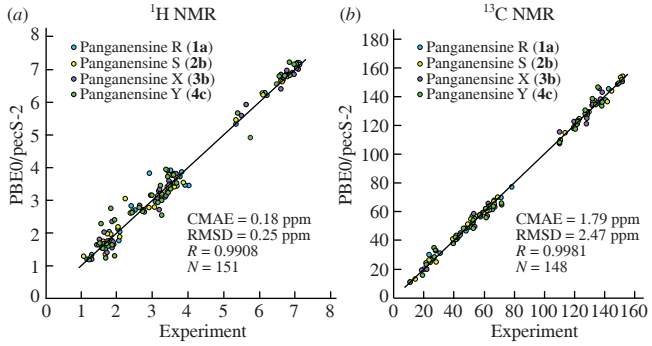

Figure 6 Correlation plots of calculated *vs*. experimental (*a*) ^{1}H NMR and (*b*) ^{13}C NMR chemical shifts (δ, ppm) for the key conformations **1a**, **2b**, **3b**, and **4c**.

On the other hand, electron density is transferred to the non-valent H-2′–H-21′ contact through the same hydrogen atom. It is these effects that eventually reflect in the value of C-2′ chemical shift.

The C-20′ chemical shift is significantly affected by its non-bonded interaction with the proton for the hydroxy group OH-17′; in this case, a bond critical point of (3,–1) type was localized between them (see Figure 5). In addition, the electronic deshielding effect of the C-19′/C-20′ π-system should also be present and properly addressed. The missing experimental ^{13}C NMR chemical shift of C-6 could be estimated based on the calculated 43.7 ppm value (see Figure S2).

As for the ^{1}H NMR chemical shifts of **3b**, all calculated values generally correlate with the experimental ones, with the exception for the proton H-2′ (Figure 6). Here, as stated above, an intramolecular hydrogen bond is formed with the oxygen atom of OH-17′, which results in the delocalization of electron density (see Figure 5). Unfortunately, it is practically impossible to take into account such interdependent stereoelectronic delocalization effects within the framework of the GIAO-DFT formalism.

In contrast to the previous case, in panganensine Y (conformer **4c**), the interaction of the OH-17′ hydroxy group with H-15 *via* oxygen atom is more pronounced, and this is reflected in larger deviation of calculated C-15 shift as compared to experiment (see Table 2). In stereoisomer Y, the C-21 atom is affected by the electron-deficient nitrogen atom N-4 due to the delocalization of the electron density of the C-20/C-21 π-system. For this reason, the calculated value for the C-21 signal is shifted upfield compared to the experiment. As for C-20′, it is influenced by the partial protonation by the hydroxy group located close the C-19′/C-20′ π-system, resulting in a discrepancy between experimental and calculated values of C-20′ chemical shift.

Chemical shifts H-14 and H-21 are affected by the electron-deficient nitrogen N-4. The H-21 chemical shift is influenced directly by the carbon bridge at C-21 (the one between N-4 and H-21 through C-21) while H-17 shift is affected indirectly *via* the through-space effect. The marked deviation between experimental and calculated values of H-17 proton shift is due to theoretical underestimation of this electronic effect.

In summary, the results of this study demonstrate that the use of an accessible computational algorithm allows performing a reliable estimation of conformational behavior of bisindole alkaloids together with configurational assignment of their asymmetric centers. In addition, the use of modern balanced basis sets allows for accurate and highly efficient prediction of shielding constants and corresponding NMR chemical shifts even in such non-trivial structures as bisindole dimeric alkaloids, as illustrated in Figure 6. To be more philosophical, this approach allows for deep penetration into the origin of spatial structure of natural products.

In general, the results of the performed study showed that the average level of error of calculated ^{1}H and ^{13}C NMR chemical shifts of natural products exemplified with four alkaloids from the root bark of *Strychnos panganensis* was essentially low. This result indicates the effectiveness of the proposed approach and the prospects for its application in the NMR spectral analysis. However, several calculated values did not fit into overall correlation and were associated with complicated stereoelectronic effects. In this communication, we attempted to clarify the reasons for these effects and determine their influence on the observed deviations.

All calculations were performed at the HPC cluster ‘Academician V. M. Matrosov’ (http://hpc.icc.ru, accessed on May 9, 2025) and at A. E. Favorsky Irkutsk Institute of Chemistry using the facilities of Baikal Analytical Center (http://ckp-rf.ru/ckp/3050, accessed on May 9, 2025).

Online Supplementary Materials

Supplementary data associated with this article can be found in the online version at doi: 10.71267/mencom.7827.

References

1 D. A. Grigoriev, V. A. Semenov, L. Angenot and L. B. Krivdin, *Int. J. Quantum Chem.*, 2024, **124**, e27323; https://doi.org/10.1002/qua.27323.
2 D. A. Grigoriev, V. A. Semenov, L. Angenot and L. B. Krivdin, *Int. J. Quantum Chem.*, 2025, **125**, e70008; https://doi.org/10.1002/qua.70008.
3 M. Frédérich, M.-J. Jacquier, P. Thépenier, P. de Mol, M. Tits, G. Philippe, C. Delaude, L. Angenot and M. Zèches-Hanrot, *J. Nat. Prod.*, 2002, **65**, 1381; https://doi.org/10.1021/np020070e.
4 N. G. Bisset and J. D. Phillipson, *Lloydia*, 1971, **34**, 1; https://pubmed.ncbi.nlm.nih.gov/5140265.
5 J.-M. Nuzillard, P. Thépenier, M.-J. Jacquier, G. Massiot, L. Le Men-Olivier and C. Delaude, *Phytochemistry*, 1996, **43**, 897; https://doi.org/10.1016/0031-9422(96)00362-7.
6 National Center for Biotechnology Information. PubChem Compound Summary for CID 44559875, S-panganensine; https://pubchem.ncbi.nlm.nih.gov/compound/S-panganensine. Accessed May 9, 2025.
7 National Center for Biotechnology Information. PubChem Compound Summary for CID 44559876, Panganensine X; https://pubchem.ncbi.nlm.nih.gov/compound/Panganensine-X. Accessed May 9, 2025.
8 Y. Zhao and D. G. Truhlar, *Theor. Chem. Account*, 2008, **120**, 215; https://doi.org/10.1007/s00214-007-0310-x.
9 Yu. Yu. Rusakov, Yu. A. Nikurashina and I. L. Rusakova. *J. Chem. Phys.*, 2024, **160**, 084109; https://doi.org/10.1063/5.0193227.
10 Yu. Yu. Rusakov and I. L. Rusakova. *J. Chem. Theory Comput.*, 2024, **20**, 6661; https://doi.org/10.1021/acs.jctc.4c00772.
11 J. Tomasi, B. Mennucci and E. Cancès, *J. Mol. Struct.: THEOCHEM*, 1999, **464**, 211; https://doi.org/10.1016/S0166-1280(98)00553-3.
12 J. Tomasi, B. Mennucci and R. Cammi, *Chem. Rev.*, 2005, **105**, 2999; https://doi.org/10.1021/cr9904009.
13 C. Adamo and V. Barone, *Chem. Phys. Lett.*, 1998, **298**, 113; https://doi.org/10.1016/S0009-2614(98)01201-9.
14 Yu. Yu. Rusakov and I. L. Rusakova, *J. Chem. Phys.*, 2022, **156**, 244112; https://doi.org/10.1063/5.0096907.
15 Yu. Yu. Rusakov and I. L. Rusakova, *Phys. Chem. Chem. Phys.*, 2023, **25**, 18728; https://doi.org/10.1039/d3cp02664g.
16 Yu. Yu. Rusakov, V. A. Semenov and I. L. Rusakova, *Int. J. Mol. Sci.*, 2024, **25**, 10588; https://doi.org/10.3390/ijms251910588.
17 Yu. Yu. Rusakov, V. A. Semenov and I. L. Rusakova, *Int. J. Mol. Sci.*, 2023, **24**, 14623; https://doi.org/10.3390/ijms241914623.
18 V. A. Semenov and L. B. Krivdin, *Russ. Chem. Rev.*, 2022, **91**, RCR5027; https://doi.org/10.1070/RCR5027.
19 D. Tavernier, M. J. O. Anteunis, M. J. G. Tits and L. J. G. Angenot, *Bull. Soc. Chim. Belg.*, 1978, **87**, 595; https://doi.org/10.1002/bscb.19780870804.
20 N. Grimblat, M. M. Zanardi and A. M. Sarotti, *J. Org. Chem.*, 2015, **80**, 12526; https://doi.org/10.1021/acs.joc.5b02396.
21 N. Grimblat and A. M. Sarotti, *Chem. – Eur. J.*, 2016, **22**, 12246; https://doi.org/10.1002/chem.201601150.
22 T. A. Keith, *AIMAll, Version 19.10.12*, TK Gristmill Software, Overland Park, KS, USA, 2019.

Received: 15th May 2025; Com. 25/7827